Hindawi
Advances in Civil Engineering
Volume 2023, Article ID 9919993, 13 pages
https://doi.org/10.1155/2023/9919993

Research Article

Research on the Deformation Law and Stress Distribution Characteristics of Overburden under the Influence of Multiple Faults

Yaobin Qi[1], **Weijian Yu**[1,2], **Desun Yu**[3], **Hanxiao Guo**[1], **and Bao Pan**[1]

[1]*School of Resource & Environment and Safety Engineering, Hunan University of Science and Technology, Xiangtan 411201, China*
[2]*Hunan Province Key Laboratory of Coal Resources Clean-Utilization and Mine Environment Protection, Hunan University of Science and Technology, Xiangtan 411201, China*
[3]*Jiujiang Vocational and Technical College, Jiujiang 332000, China*

Correspondence should be addressed to Yaobin Qi; 15731808725@163.com

Received 7 July 2023; Revised 1 October 2023; Accepted 16 October 2023; Published 14 November 2023

Academic Editor: Wei-yao Guo

Taking the geological conditions of a coal mine in Liupanshui City, Guizhou Province, as the background. The fracture law of the roof in the coal face and the height of the "Two zones" were obtained through theoretical analysis and empirical formula calculation, and the results were verified using similar simulation experiments. Through numerical simulation were researched the stress distribution characteristics of the overlying strata on the working face under the influence of multiple faults. The results showed that in the early stage of mining, F1 undergoes activation under the influence of the main roof weighting, leading to an increase in the degree of plastic damage to the coal seam and strata behind the working face, causing a redistribution of the behind abutment pressure. Finally, under the influence of the F1 barrier effect, the vast majority of the behind abutment pressure is transferred to the lower strata of F1, leading to a continuous increase in stress concentration there. But as the working face continues to advance, the blocking effect of the roof plastic zone above the goaf on the transmission of the behind abutment pressure of the working face begins to appear and continues to increase, leading to a decrease in the peak stress at the lower strata of F1. The stress change process on the F2 side is similar to that on the F1 side, the front abutment pressure is initially distributed in the strata in front of the working face, but as the activation degree of F2 continues to intensify, it gradually shifts to the lower strata of F2, and ultimately the majority of the front abutment pressure is borne by the lower strata of F2.

1. Introduction

The international situation is complex and changeable, and the importance of energy is becoming increasingly prominent, resulting in the demand for coal worldwide increasing yearly. In order to meet the needs of national construction and improve coal output, it is necessary to study coal mining under complex geological conditions. Many scholars have conducted research in different directions, such as deep coal mining [1–3], coal mining in fault-affected areas [4–6], underground mining of thin coal seams [7–9], and mining under hard roof conditions [10–12]. In these mining conditions, the fault is exceptional. The existence of faults can cut through the original strata, causing a diminution in the integrity and continuity of the strata. Moreover, the density of the rock mass in the fault area is small, and there are many cracks, which will make its barrier effect more visible, resulting in abnormal stress concentration in the overburden of the coal face, the deformation and destruction of the roof intensified, roof fall, spalling, rock burst, and other disasters occur frequently.

In order to solve some problems encountered during the mining process in areas affected by faults, many scholars have done much research. Bai et al. [13] obtained two stages of delayed water inrush evolution in fault fracture zones by analyzing examples of delayed water inrush from faults. Zhang et al. [14] used UDEC to assay the impression of distinct fault spacing and mining directions on the variant

of overlying strata during mining in a dual fault area. The relationship between fault activation and dynamic response was obtained, and the experimental results were verified through microseismic monitoring data. Jiao et al. [15] obtained through numerical simulation that the coal mass around the fault will accumulate elastic strain energy due to the influence of the fault and thick roof and increase the rock burst vitality. Lan et al. [16] revealed the relationship amid fault construction and mining engineering by classifying the fault construction forms of rock bursts and establishing geological structure models. Zhang et al. [17] investigated the danger dimension of water inrush from faults at different locations by establishing a fluid–structure coupling analysis model and a numerical model. Wang et al. [18] verified the characteristics of roof stress sudden change under the joint action of double faults employing field monitoring and similar simulation and revealed the mechanism of irregular fracture of roof strata. Danesh et al. [19] used numerical simulations based on actual situations to obtain several factors that can predict the final stress state. Kong et al. [20] found that the high normal stress level of the reverse fault during coal mining will cause an increase in the shear strength of the reverse fault, and the sliding displacement of faults is affected by the size of the coal pillars. Guo et al. [21] investigated the factors that exacerbate fault activation and found that fault activation increases the barrier effect on stress distribution. Kruszewski et al. [22] developed a static 3D geomechanical model using a large amount of raw data obtained during long-term mining processes to prognosticate the spatial consecutive distribution of unmolested in situ stress states and assess the reactivation danger of the main fault zone. Islavath et al. [23] provided two practical methods for dividing the panel into two subpanels to transmit faults and proposed that in order to elevate the fixity of the coal face, it is needful to avoid the emergence of the goaf when the long wall face is close to the fault. Wang et al. [24] investigated the movement particularities of hard and thick strata under the influence of faults and the impact of mining direction on fault slip and obtained two rock burst-induced modes and occurrence mechanisms. Also, the construction of the overlying layers on the two fault walls will be involved by fault cutting and fault dip angle. Zhang et al. [25] obtained the rock mass parameters of fault zones that have a significant impact on fault activation through numerical simulation methods, as well as the degree to which changes in the size of these parameters affect fault activation. Tan et al. [26] researched the impact of faults on crustal stress at different positions of faults through hydraulic fracturing tests and revealed the reasons for the different distribution of crustal stress near faults through numerical simulation. Finally, the focal mechanism solution was verified. Dou et al. [27] studied the earmarks of the initial stress realm and the mining stress realm, as well as the coupling effect between them. Also, analyzed the connection between the regional stress field and earthquake events and coal explosions and proposed stress field control methods for preventing coal and rock explosions. Chen et al. [28] utilized numerical simulation to obtain the range of fault dip angles that can easily cause fault activation, as well as the nexus between fault drop and water inrush disasters. Zhang et al. [29] obtained the mechanical parameters of the rock samples through indoor experiments and used numerical models to analyze the relationship between coal seam thickness and wave shape, as well as several factors affecting wave formation. Wang et al. [30] identified several main factors leading to roadway instability through research on mine monitoring data and examples, and a new support scheme was proposed based on adherence to the support principles, which was verified through on-site testing afterward.

Most previous studies considered the influence of a single fault, but the study on the migration law and stress distribution characteristics of roof strata in multifault-affected areas is relatively small. In order to solve this problem, this paper studies the collapsed shape, fracture rule, and vertical stress distribution characteristics of overlying strata in multifault-affected areas by theoretical calculation, similar simulation experiments, and UDEC numerical simulation. It provides a reference basis for mining under the influence of multiple faults.

2. Project Overview

The mining area of a coal mine in Liupanshui City covers an area of 1,45,526 m^2, and the selected coal face is situated in the western region of Mining Area 21. Its starting point is the 212 and 213 transportation cross-cuts in the east, and its endpoint is the setup entry in the west, and the upper section is 21,127 goaf. Other mining does not influence the mining of this coal face. No buildings are on the surface, and no other projects are affecting the stopping.

There are two layers of coal in this mining area. The main minable coal seam is 12#, with a maximum burial depth of 360 m and an average buried depth of 326 m. The average thickness of the coal seam is 5 m. It pertains to a flat seam. The coal face adopts the long wall mining. Full-thickness mining at one time. Using the full collapse method to manage the roof. The 12# coal seam is stable in occurrence, simple in structure, layered—massive in structure, grayish black, semibright, brittle, loose, and fragile at the bottom. The coal face is penetrated by two faults that are relatively close to each other. These two faults are reverse fault F1 with a dip angle of 45° and throw height of 5 m and normal fault F2 with a dip angle of 45° and throw height of 5 m. See Figure 1 for the distribution of strata in the mining area.

3. Migration Characteristics of Roof Strata in Multifault Areas

3.1. Breaking the Law of the Main Roof. Assuming that the overburden load is uniformly distributed, the magnitude of the main roof overburden load q can be obtained according to the combined beam theory [31].

$$(q_n)_1 = \frac{E_1 h_1^3 (\gamma_1 h_1 + \gamma_2 h_2 + \cdots + \gamma_n h_n)}{E_1 h_1^3 + E_2 h_2^3 + \cdots + E_n h_n^3}. \quad (1)$$

There are often several thick and hard strata in the overburden of the working face, due to the deflection of thick and

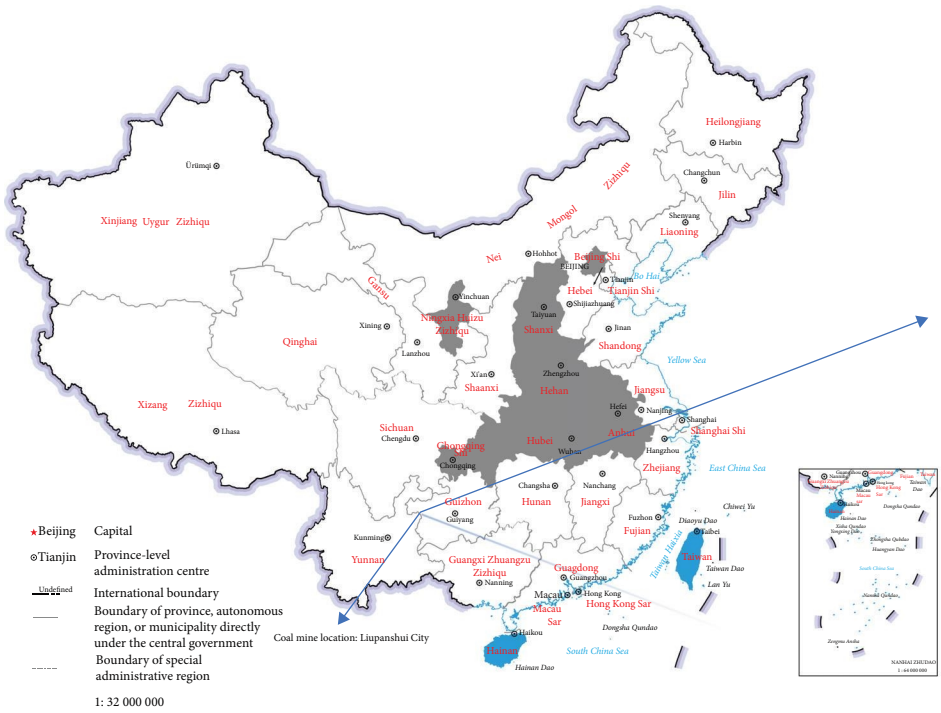

Columnar	Lithology	Thickness (m)
	Siltstone	26
	Fine sandstone	5
	Calciferous sandy claystone	4
	Siltstone	22
	Calciferous sandy claystone	6
	Fine sandstone	8
	Siltstone	3
	Silty claystone	4
	Coal seam 12#	5
	Silty claystone	5
	Fine sandstone	7
	Coal seam 13-2#	5
	Calciferous sandy claystone	20

FIGURE 1: Geological histogram.

hard strata is smaller than that of the lower strata [31], the strata below it no longer needs to bear the load brought by other strata above it. Therefore, according to the composite beam theory, assuming that the load in the strata is uniformly distributed, if the $n+1$ layer is a thick and hard stratum, then:

$$(q_{n+1})_1 < (q_n)_1. \tag{2}$$

First, starting from the first strata above the coal seam, calculate the parameters in Table 1 by substituting them into Equation (1) to determine the position of the first thick and hard stratum. Because the main roof is located above the immediate roof, it is generally thick, hard, and has strong integrity. Its characteristic is that it does not collapse on its own after returning to the column and often only slowly sinks. The first thick and hard stratum precisely conforms to these characteristics of the main roof, so this article will use it as the main roof for research. After determining the main roof, use Equation (1) to recalculate from the first thick and hard stratum, and use Equation (2) to distinguish, find the second thick and hard stratum, and the magnitude of the overlying load q of the main roof studied in this study can be obtained, thus obtaining the fracture law of the main roof. The specific calculation steps are as follows:

Substituting the parameters in Table 1 into Equation (1) can obtain the self-load of the first layer of silty mudstone above the coal seam as follows:

$$q_1 = \gamma_1 h_1 = 19.8 \times 4 = 79.2\ (\text{kPa}). \tag{3}$$

The loading action of the second layer on the first silty mudstone is as follows:

$$(q_2)_1 = \frac{E_1 h_1^3 (\gamma_1 h_1 + \gamma_2 h_2)}{E_1 h_1^3 + E_2 h_2^3} = 103.5\ (\text{kPa}). \tag{4}$$

The loading effect of the third layer on the silty mudstone of the first layer is as follows:

$$(q_3)_1 = \frac{E_1 h_1^3 (\gamma_1 h_1 + \gamma_2 h_2 + \gamma_3 h_3)}{E_1 h_1^3 + E_2 h_2^3 + E_3 h_3^3} = 35.05\ (\text{kPa}) < (q_2)_1. \tag{5}$$

From the above calculation results, it can be seen that the third layer of fine sandstone above the coal seam has no effect on the load of the first strata and can be regarded as the first thick and hard stratum (the main roof). The next calculation starts from the first thick and hard stratum and repeats the above process to determine the magnitude of the overlying load on the first thick and hard stratum. The specific calculation steps are as follows:

By incorporating the parameters into Equation (1), the self-load of the first thick and hard stratum can be calculated as follows:

$$q_1 = \gamma_1 h_1 = 212.8\ (\text{kPa}). \tag{6}$$

Table 1: Calculation parameters of rock stratum load.

Rock stratum	Lithology	Thickness (m)	Body force (kN/m³)	Modulus of elasticity (GPa)
1	Silty claystone	4	19.8	14.2
2	Siltstone	3	24.6	16.1
3	Fine sandstone	8	26.6	15.9
4	Calciferous sandy claystone	6	19.8	14.2
5	Siltstone	22	24.6	16.1

When calculating to the second layer, the load of the first thick and hard stratum is as follows:

$$(q_2)_1 = \frac{E_1 h_1^3 (\gamma_1 h_1 + \gamma_2 h_2)}{E_1 h_1^3 + E_2 h_2^3} = 240.85 \text{ (kPa)}. \quad (7)$$

When calculating to the third layer, the load of the first thick and hard stratum is as follows:

$$(q_3)_1 = \frac{E_1 h_1^3 (\gamma_1 h_1 + \gamma_2 h_2 + \gamma_3 h_3)}{E_1 h_1^3 + E_2 h_2^3 + E_3 h_3^3} = 38.9 \text{ (kPa)} < (q_2)_1, \quad (8)$$

where E—elastic modulus of rock layer; h—depth of stratum; γ—unit weight of rock layers.

From the calculation results, it can be seen that the third layer of siltstone has high strength and thick stratum, which have no effect on the load of the first thick and hard stratum. It can be regarded as the second thick and hard stratum. Therefore, only the load effect of the second layer (calciferous sandy clay stone with a height of 6 m) on the first thick and hard stratum needs to be considered. From this, it can be determined that the overlying load of the first thick and hard stratum (the main roof) is $q = 0.24085$ MPa.

During the mining duration of the coal face, the main roof will be in a suspended state after the immediate roof is entirely collapsed. Although the overlying strata are cut by F1 and F2 and become discontinuous, our research object is the rock stratum between the two faults, and during mining, the protective coal pillars with specified lengths are reserved on both sides of the coal face, so the main roof can still be regarded as a beam with two ends constrained. The fracture of the main roof is analyzed by using the fixed beam model in elastic mechanics.

As shown in Figure 2, the stress distribution of the fixed beam is symmetrical, so in the middle of the beam, the shear stress is zero, the normal stress on the transversal surface of the beam is the transverse principal stress σ_1, and the tensile stress σ_1 reaches the maximum at $(0, h/2)$ [32] as follows:

$$\sigma_{1\max} = \sigma_x \Big|_{\left(0, \frac{h}{2}\right)} = \frac{q}{5} + \frac{ql^2}{h^2}. \quad (9)$$

According to the maximum tensile stress criterion, the ultimate span of a beam that does not undergo fracture must meet the following:

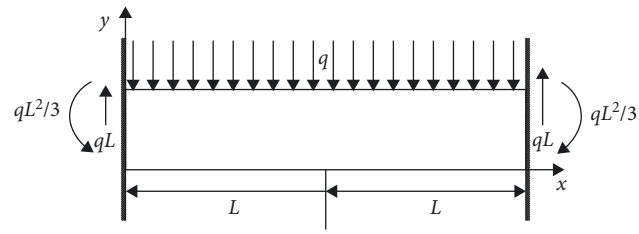

Figure 2: Force analysis of fixed beam model.

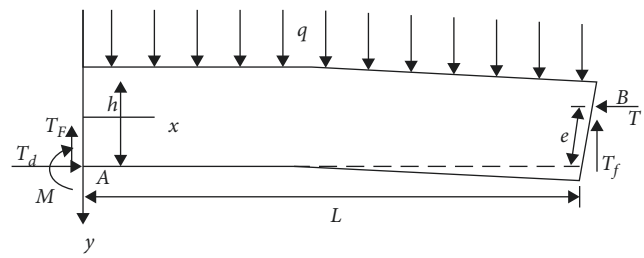

Figure 3: Force analysis of cantilever beam model.

$$\sigma_{1\max} = \frac{q}{5} + \frac{ql^2}{h^2} \le [\sigma]. \quad (10)$$

From this, it can be seen that the ultimate safe span for the first break of the fixed beam is as follows:

$$L_s \le 2h\sqrt{\frac{[\sigma]}{q} - \frac{1}{5}} = 45.5 \text{ (m)}, \quad (11)$$

where L_s—first weighting interval of the main roof; h—height of the main roof, 8 m; $[\sigma]$—ultimate tensile strength of the main roof, 2.0 MPa; q—load on the main roof.

After the main roof is broken, the roof strata will be in a state where one end is constrained, and the other end is suspended, so the cantilever beam model in elastic mechanics can be used to analyze the roof breakage.

As shown in Figure 3, the expression of the stress component in the cantilever beam is the same as that of the fixed beam, but the boundary constraint conditions are different, so the safety limit span of the cantilever beam can be obtained by substituting the boundary conditions of the fixed end and free end of cantilever beam [32] as follows:

Stress monitoring system

Leica TZ12 total station

Similar simulation test-bed

Figure 4: Experimental equipment.

$$-\frac{q}{2}-\left(\frac{6Te}{h^2}-\frac{3ql^2}{h^2}-\frac{3T}{h}-\frac{3q}{10}\right)-\frac{T}{h}\le[\sigma]. \tag{12}$$

From this, it can be seen that the safety limit span for cantilever beam breaking is as follows:

$$L_Z=\sqrt{\frac{5h^2[\sigma]+qh^2+30Te-10Th}{15q}}=13.6\ (\mathrm{m}), \tag{13}$$

where L_z—periodic weighting interval of the main roof; T—horizontal thrust, here 0.

3.2. The Height of the "Two Zones". When using the full collapse method to manage the roof, the overburden can be divided into three zones pursuant to the movement and destruction degree of the overburden, in which the strata with irregular caving and significant loose coefficient are the caving zones. The rock stratum above the caving zone, regularly broken and with a small coefficient of breaking expansion, is called the fractured zone.

The saturated uniaxial compressive strength of the rocks in the overburden is 20–40 MPa, belonging to medium hard rock, which can be calculated pursuant to the following formula [33]:

$$H_c=\frac{100M_h}{4.7M_h+19}\pm 2.2=9.56-13.96\ (\mathrm{m}), \tag{14}$$

$$H_f=\frac{100M_h}{1.6M_h+3.6}\pm 5.6=37.5-48.7\ (\mathrm{m}), \tag{15}$$

where H_f—height of the fractured zone; H_c—height of the caving zone; M_h—mining height, the value here is 5 m.

4. Similarity Simulation Experiment of Overlying Strata Migration

4.1. Experimental Equipment and Similarity Constants. According to the experimental conditions, a multifunctional plane and 3D similar material simulation test bed with the size of length × width × height = 2,500 × 300 × 1,500 mm were selected. The model laying height was 1,200 mm, and the overlying non-simulated strata were replaced with bricks of the same weight.

According to the actual needs of the study and the similarity law, the similarity constant of this test is determined as follows: the geometric similarity constant is 100, the time similarity constant is 10, the volume weight similarity constant is 1.5, and the stress similarity constant is 150. *Leica TZ12* total station is used for displacement monitoring, and the *DH3816N* strain gauge is used for the stress monitoring system. All instruments are tested before the experiment to ensure no error. The equipment used in this experiment is shown in Figure 4

4.2. Experimental Materials and Proportions. The 2D similar model established in the background of mine geological conditions can well reflect the deformation law of the overburden. The proper and reasonable option of similar materials and material proportions is the critical condition for the success of the experiment. By summarizing the research of other scholars and combining the characteristics of the material itself, this experiment finally selects river sand as aggregates and lime and gypsum as cement. In that proportion, the main strength index is the compressive strength. The main deformation index is the elastic modulus and Poisson's ratio. Pursuant to the study of Wu et al. [34], the proportion of materials and rock mechanics parameters that can meet the experimental requirements are shown in Table 2.

According to the determined ratio, calculate the amount of each layer of material, mix all kinds of materials evenly, add water with a weight of 1/10 of the material weight, and quickly stir evenly to prevent caking. Pour the mixed material into the model, scrape and compact the surface to a thickness that meets the calculated layer thickness, and

Table 2: Rock mechanics parameters.

Ground	Density (kg/m³)	Cohesion (MPa)	Friction angle (°)	Poisson's ratio	Elastic modulus (GPa)	Compressive strength	Tensile strength (MPa)	Ratio number[a]
Siltstone	2,460	3.2	30	0.23	16.1	40.2	2.4	355
Fine sandstone	2,660	2.2	32	0.25	15.9	32.8	2.0	437
Silty claystone	1,980	0.7	26	0.21	14.2	30.5	1.7	455
12coal seam	1,620	0.6	22	0.37	2.4	22.0	0.2	637
13-2coal seam	1,620	0.6	22	0.35	2.7	18.0	0.23	637
Calciferous sandy claystone	1,980	0.7	26	0.21	14.2	30.5	1.7	455

Note. [a]Ratio number: the ratio of aggregate to binder. For example, the meaning of "637" is 6 : 1(3 : 7), which means that when making a model, the ratio of aggregate to binder is 6 : 1; in the binder, the ratio of lime to gypsum is 3 : 7.

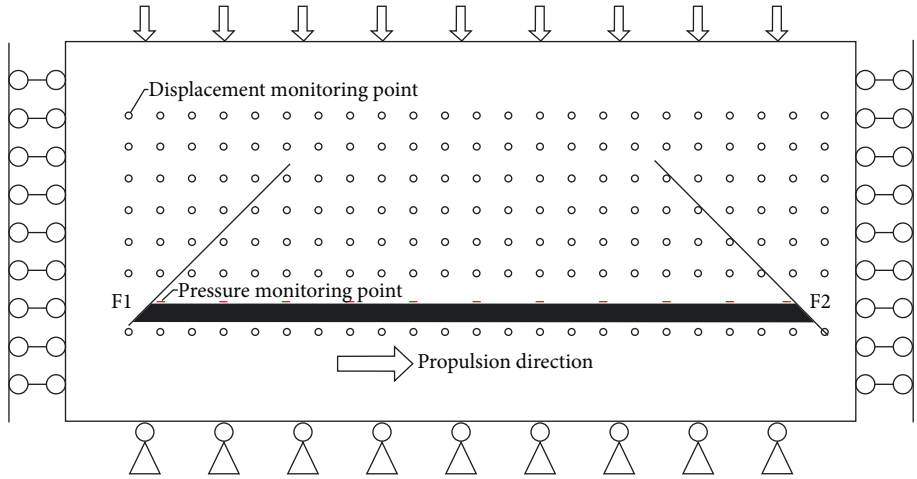

Figure 5: Location of measuring points.

sprinkle a layer of mica powder on each material layer to simulate the joint surface between strata. Due to the faults in the model, the steel plates were adjusted to the required angle and fixed when laying the model and the middle part was laid first, and then the steel plates were removed and laid on both sides. After standing for one week, remove the baffle and start the test after 20 days.

4.3. Monitoring Plan. In order to facilitate monitoring of changes in roof layer displacement, the model's surface was painted white, and the coal seam was painted black after the model was laid. Using the upper boundary of the coal seam as the benchmark, we use the ink box for popping up uniform grid lines in the horizontal and vertical directions on the model surface, and the intervals between the lines are 10 cm. The reflector is pinned at the intersection of the grid lines to observe and record the displacement of the strata.

To study the alterations of front abutment pressure during the mining process, place the strain gauge in the strata 2 cm above the coal seam for registering, start placing at 5 cm to the right of F1, strain gauge spacing 20 cm, placed a total of 11, from left to right in accordance with the 1–11 number, this step should be completed in the laying model, stress sheet wrapped with plastic wrap to prevent water damage. See Figure 5 for a specific arrangement.

4.4. Model Mining and Analysis of Experimental Results. In the experimental model, 30 cm protective coal pillars are reserved for both F1 and F2. The length of the coal seam mined in the simulation experiment is 150 cm, and the actual mining length is 150 m. Starting mining at 30 cm on the right side of F1. Each time is advanced by 5 cm, and the excavation is carried out 30 times. The interval of each excavation is 0.5 hr. The time effect of surrounding rock deformation is considered. The deformation of overlying strata during mining is shown in the figure below.

Figure 6 shows the movement of overburden and the expansion of fractures at different mining stages. From the figure, we can see that when the coal seam is excavated for 20 m, there is no variant of the roof, but fissures have been generated in the overburden, and the expansion height of the fissures is 4 m. When the coal seam is excavated for 25 m, the immediate roof collapses for the first time, the initial caving step is 25 m, the caving height is 5 m, and the goaf can not be filled entirely. Later, as the excavation of the coal seam reaches 25–45 m, the immediate roof collapses with mining, the caving height reaches 7 m, and the cracks in the overburden develop continuously upward. When the coal seam is excavated for 45 m, the main roof is broken, and the first weighting interval is 45 m. Because of the rain for several days before the experiment, the model becomes damp and its strength decreases, so the main roof did not form an apparent masonry block structure after the first weighting.

When the coal seam is excavated for 62 m, the first periodic weighting occurs on the main roof, and the weighting interval is 17 m. After the main roof breaks, the apparent masonry block hinge structure is formed, and the transverse crack appears 5 m above the main roof and extends to the front of the working face. When the coal seam is excavated for 105 m, the main roof appears the fourth periodic weighting, and the strata subsidence at 5 m above the main roof leads to strata separation with a length of 30 m. The coal seam continues to be excavated, and the fracture continues to expand forward, but the length of the separation layer does not increase. Also, with the overall subsidence of the overlying strata, the separation layer gradually closes, and the length of the separation layer gradually decreases. When the coal seam was excavated for 150 m, the mining was completed. During this period, the main roof was periodically weighted seven times. The maximum weighting step was 17 m, the minimum was 13 m, and the average periodic weighting interval was 15 m.

Figure 6(e) is the final state of the model. It can be seen that the coal rib support area is formed above the unexcavated coal seam, the separation area is formed on both sides of the excavated part, and the collapsed rock is recompacted in the middle part due to the downward movement of the roof strata, and the original cracks are closed to form the recompaction area. A 90 m-long separated layer fracture appears 40 m above the coal seam. The strata below the fracture form a fractured zone and a caving zone from top to bottom.

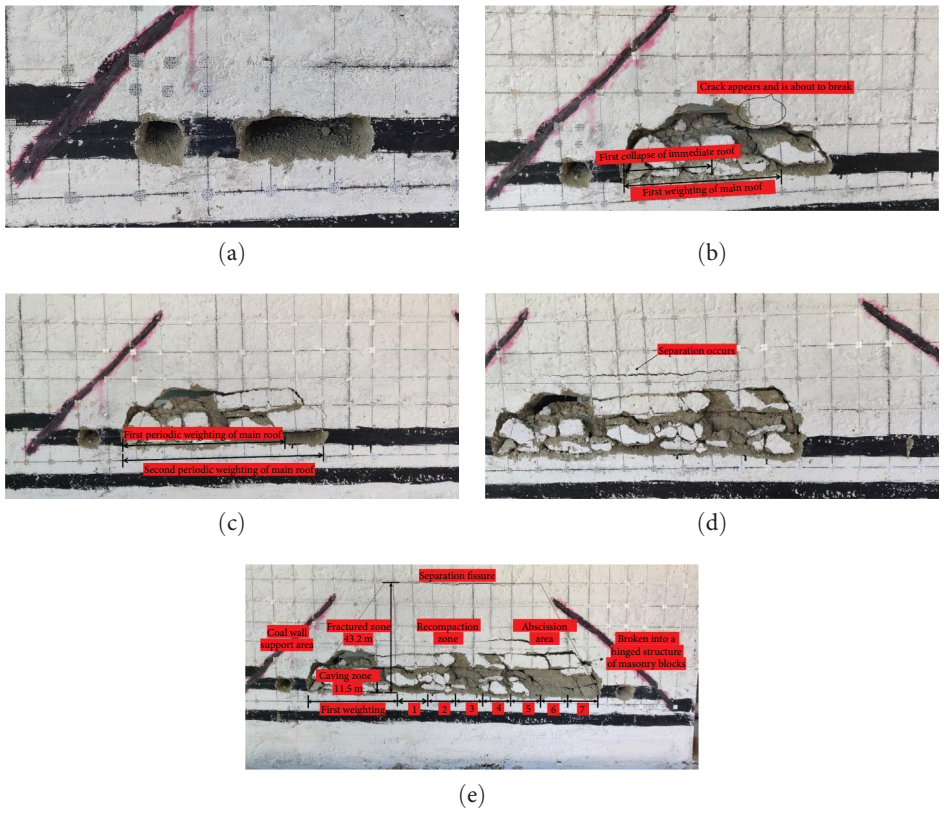

Figure 6: Coal seam advancing process: (a) excavated 20 m; (b) excavated 60 m; (c) excavated 75 m; (d) excavated 105 m; (e) end of excavation.

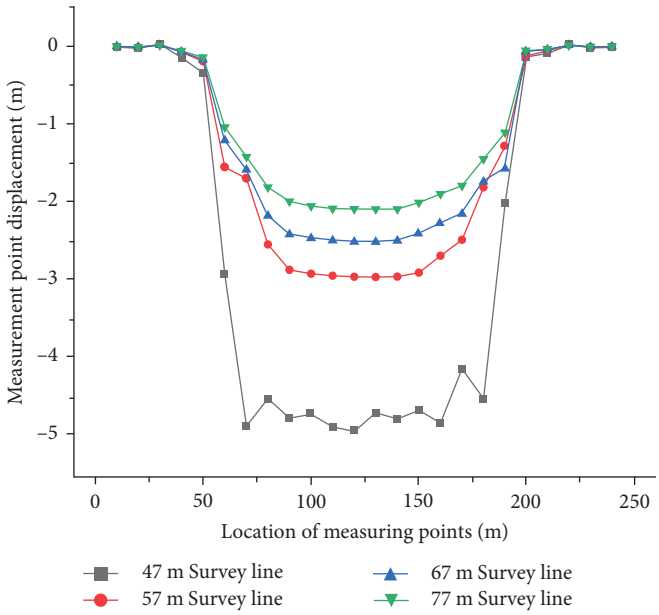

Figure 7: Displacement change diagram of monitoring points.

The height of the caving zone is 11.5 m, and the height of the fractured zone is 43.2 m. As shown in Figure 7, the displacement fluctuation of the measuring points on the 47 m monitoring line is significant, and the change is highly irregular, which indicates that the rock stratum in this layer belongs to the caving zone. However, the displacement curves of the measuring points at 57, 67, and 77 m are relatively continuous. The rock layers of the three layers change cooperatively with little difference, which conforms to the change earmarks of the strata in the fractured zone.

The breaking span of the main roof and the height of the "Two zones" obtained by the similar simulation experiment are accordant with the theoretical calculation results, which can furnish a reference for the production of mines under analogous circumstances.

5. Numerical Simulation Analysis of Mining in Multifault Area

5.1. Modeling. Based on the geological data of a coal mine in Liupanshui City, the vertical stress distribution characteristics of the surrounding rock under the influence of multifault are analyzed using the UDEC, and the Mohr–Coulomb yield criterion and Coulomb slip model of surface contact are adopted. The model size is set as length × height = 250 × 120 m (see Figure 8), including reverse fault F1 and normal fault F2 from left to right, the dip angle of the fault is 45°, the offset is 5 m, and the fault in the model is represented by a weak fracture belt with a width of 1 m. In this experiment, the mining of 12# coal seam is simulated, the inclination angle is set to 0, and the buried depth is $H = 326$ m, so apply a gradient in situ vertical stress of 5.6–8.4 MPa from top to bottom inside the model. Also, set the lateral pressure coefficient to 1.2 based on

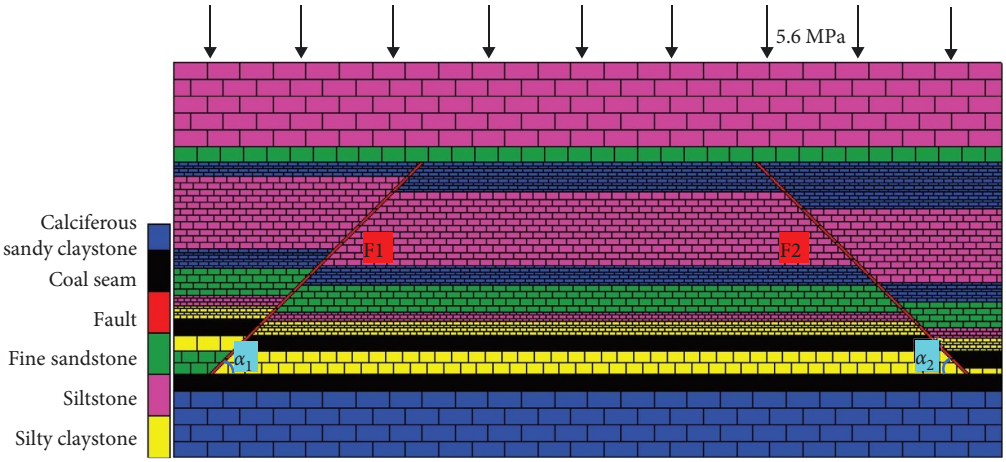

Figure 8: Numerical model diagram.

the burial depth and apply gradient in situ horizontal stress of 6.7–10.1 MPa from top to bottom inside the model.

Apply a downward force of 5.6 MPa to the margin at the top of the research model to replace the unmodeled strata. Both sides of the model can move vertically but not horizontally, and the margin bottom of the research model can move horizontally but not vertically. The rock mechanics parameters used for numerical analysis are the same as in Table 2.

5.2. Vertical Stress Distribution Characteristics of Overburden in Working Face

5.2.1. Vertical Stress Nephogram and Monitoring Line Location. According to the experimental needs, the vertical stress cloud chart of the surrounding rock of stope under six different advancing lengths of 20 m, 25 m (first caving of the immediate roof), 45 m (first weighting of the main roof), 62 m (first periodic weighting of the main roof), 105 m (fourth periodic weighting of the main roof), and 150 m (completion of mining) is selected (see Figure 9, Unit: Pa), to analyze the variation law of vertical stress of the overburden.

A 200 m long stress monitoring line is arranged in the 12# coal seam, starting from the setup entry and ending at the right boundary of the model. Export the obtained data to obtain the change curve of the front abutment pressure of the coal face (see Figure 10). According to the curve, the remit and peak position of the front abutment pressure can be obtained.

5.2.2. Numerical Simulation Results. With the advance of the coal face, the overburden in the goaf will appear as an evident stress zoning phenomenon, which is generally divided into tensile stress area, compressive stress concentration area, pressure relief area, and compression area [35]. In the pressure relief area, the vertical and horizontal stresses are below the in situ stress level. Nevertheless, in the compression region, the vertical stress decreases, and the horizontal stress increases. Therefore, the height of the pressure relief arch above the goaf can be determined by the changes in the magnitude of vertical and horizontal stresses.

Combining Figures 9 and 10, it can be seen that when the coal seam is excavated to 20 m, the roof above it does not collapse, and the stress concentration phenomenon occurs on both sides of the goaf. The stress concentration of the strata on the left side exceeds that on the right side, and the stress concentration phenomenon is more evident for the strata close to the fault. In the lower strata of F1, there is also an extensive range of stress concentration phenomena. The pressure relief arch is 15 m from the upper boundary of the goaf, and the influence limit of the front abutment pressure is 60 m in front of the working face.

When the coal seam is excavated to 25 m, the stress concentration degree on the left hand of the goaf decreases, the stress begins to accumulate in the rock layers near the fault, and at the same time, the stress concentration in the lower layer of F1 increases and distributes in a concentric circle. Among them, the stress concentration amplitude in the lower end of F1 is the highest, with a stress concentration coefficient of 1.94, and the outer ring decreases in turn. The height of the pressure relief arch is 33 m at the upper boundary of the goaf, and the influence limit of the front abutment pressure is 78 m in front of the coal face. At this time, F2 has not yet been affected by mining, and the surrounding rock layers are still in the original rock stress state.

When the coal seam is excavated to 45 m, the immediate roof collapses with mining, the stress concentration degree at the lower strata of F1 continues to increase, and the stress concentration coefficient reaches around 2.9. The stress concentration at the left protective coal pillar in the goaf disappears, and the pressure of the surrounding strata is relieved. The pressure relief arch is 54 m away from the margin top of the goaf, and the influence extent of the front abutment pressure is 80 m in front of the working face. At this point, F2 began to be affected by mining and became more active. Some of the strata below it near the coal seam underwent plastic failure and pressure relief, and the stress concentration occurred on the right side of F2.

When the coal seam is excavated to 62 m, the coal and rock mass on the left side of the goaf still appear to be pressure relief, the stress concentration degree of the lower

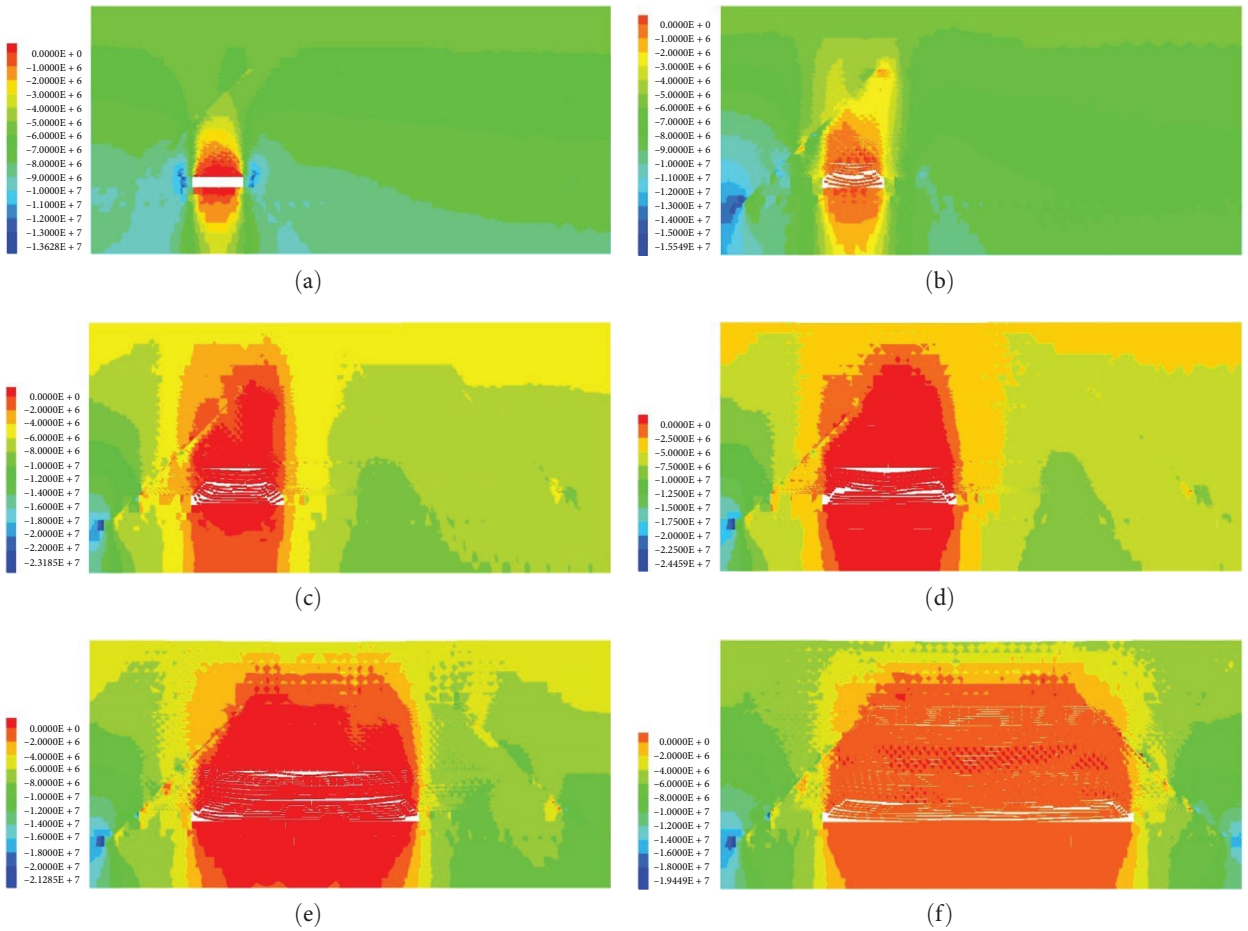

Figure 9: Cloud diagram of vertical stress distribution of overlying strata in multifault area: (a) excavated 20 m; (b) excavated 25 m; (c) excavated 45 m; (d) excavated 62 m; (e) excavated 105 m; (f) excavated 150 m.

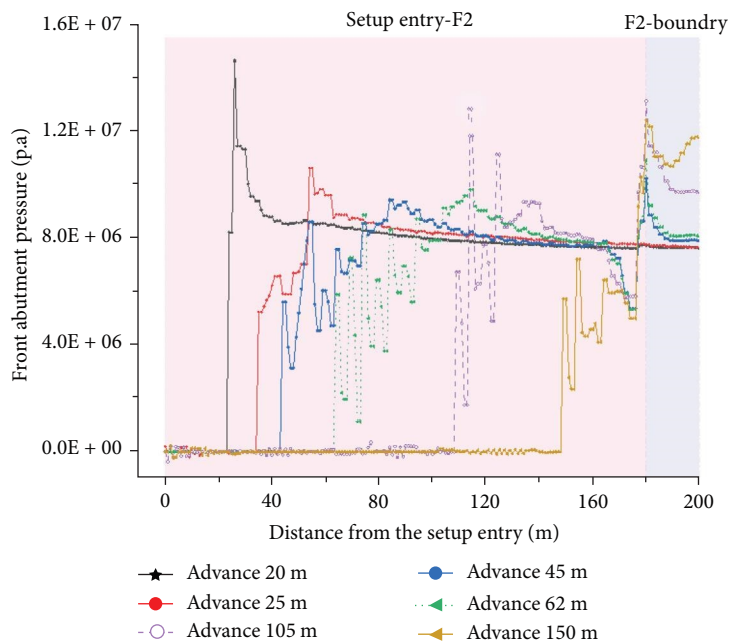

Figure 10: Curve diagram of the front abutment pressure variation in multifault area mining.

strata in F1 continues to increase, and the stress concentration coefficient reaches 3.06. The peak stress at the right strata of F2 is also continuously increasing. The pressure relief arch is 58 m away from the margin top of the goaf, and the influence extent of the front abutment pressure is 83 m in front of the working face.

When the coal seam is excavated to 105 m, the separation layer appears 19 m above the gob. The stress concentration coefficient of the lower strata of F1 decreases to 2.66. However, there is a large-scale stress concentration in the lower strata of F2, and the peak stress continues to increase. The pressure relief arch is 69 m away from the margin top of the goaf, and the influence extent of the front abutment pressure is 51 m in front of the working face.

When the coal seam is excavated to 150 m, the mining is finished, most of the roof and floor are in a state of pressure relief, and the pressure relief arch is 76.5 m away from the margin top of the gob. At this time, the stress concentration area at the lower strata of F2 is similar to that at the F1 side and presents concentric circular diffusion. However, the stress peak and strata pressure relief range on the F1 side are higher than those on the F2 side.

5.2.3. Analysis of Experimental Phenomena. After analyzing the experimental phenomena described above, it can be obtained that after the main roof stratum is broken, a portion of the mining-induced stress is transmitted to the rear of the working face. However, due to the influence of F1 activation and coal seam mining, a large area of plastic damage occurs in the strata behind the working face. Resulting in a redistribution of the behind abutment pressure and transfer to the strata on the left and lower of F1, where plastic failure did not occur. However, the former is affected by the blocking effect of F1, and only a small part can be transferred to the left strata of F1. So, ultimately, the majority of the behind abutment pressure is transferred to the lower strata of F1, resulting in a sharp increase in stress concentration at that location.

However, due to the continuous deformation and fracture of roof strata, the scope of the plastic zone above the goaf is increasing, and the plastic zone also has a blocking effect on the transmission of the mining-induced stress on the working face. After the working face is advanced to a certain distance, the blocking effect begins to appear, causing the peak stress at the lower strata of F1 to decline. With the continuous advance of the working face, the impact of mining on F2 is becoming more and more obvious, and its activation level is increasing, exacerbating the plastic deformation and damage of the coal seam and strata in front of the working face. Resulting in a redistribution of the front abutment pressure, transferring to the strata on the right and lower of F2 where plastic failure did not occur. However, the former will also be affected by the blocking effect of F2, so eventually, most of the front abutment pressure is transferred to the lower strata of F2, resulting in the scope of stress concentration area is continuously expanded and the peak value of stress is continuously increased. Throughout the entire mining process, F1 and F2 have gone through three stages of initial stabilization–activation–restabilization, and the lower strata of both faults bear a portion of the mining-induced stress of the working face. Among them, the stress borne by the lower strata of F1 is large and long-lasting, playing a major role.

It ought to be heeded that when the coal seam is excavated to the 25–62 m section, the stress concentration degree at the lower strata of F1 continues to increase. In combination with the above, the presence of F1 and F2 will flare the metamorphosis and damage of the roof, so under the joint influence of severe surrounding rock movement and large area and high-strength stress concentration, It is highly likely to intensify the activation of faults, increase their slip amount and release a large amount of energy to provide dynamic loads, and finally lead to the occurrence of rock burst. Therefore, attention shall be paid to predicting and preventing rock bursts during mining. Prevent accidents from happening.

6. Conclusions

(1) The height range of the "Two zones" in the overburden was calculated through empirical formulas and verified in similar simulation experiments. Finally, the height of the caving zone was determined to be 11.5 m and the height of the fractured zone to be 43.2 m

(2) A similar simulation experiment obtained the caving law of overburden in the multifault areas. In the mining process, the first caving step of the immediate roof is 25 m, the first weighting interval of the main roof is 45 m, and the average periodic weighting interval is 15 m, which is consistent with the theoretical calculation results. During the mining period, there are seven times periodic weightings. After mining, the overburden of the coal seam formed "Two zones" in the vertical direction and "three areas" in the horizontal direction.

(3) In the early stage of mining, F1 undergoes domestication under the influence of main roof weighting, leading to an increase in the degree of plastic damage to the coal seam and strata behind the working face, causing a redistribution of the behind abutment pressure. Finally, under the influence of the F1 blocking effect, the vast majority of the behind abutment pressure is transferred to the lower strata of F1, leading to a continuous increase in stress concentration there. But as the working face continues to advance, the blocking effect of the roof plastic zone above the goaf on the mining-induced stress of the working face begins to appear and continues to increase, leading to a decrease in the peak stress at the F1 lower strata. The stress change process on the F2 side is similar to that on the F1 side. The front abutment pressure is initially distributed in the strata in front of the working face, but as the activation degree of F2 continues to intensify, it gradually shifts to the lower strata of F2, and ultimately, the majority of the front abutment pressure is borne by the lower strata of F2.

During the entire mining process, the lower strata of F1 plays a major role in bearing the mining-induced stress of the working face.

(4) When the coal seam is excavated to the 25–62 m section, the stress concentration degree at the lower rock stratum of F1 continues to increase, and the existence of F1 and F2 can aggravate the deformation and failure of the overlying strata. Finally, under the joint action of high stress and severe surrounding rock deformation may induce rock burst in the working face or adjacent roadway, so the prediction and prevention shall be strengthened.

Data Availability

The experimental data used to support the findings of this study are available from the corresponding author upon request.

Conflicts of Interest

The authors declare that there are no conflicts of interest regarding the publication of this article.

Authors' Contributions

Conceptualization was done by Yu WJ; methodology was done by Qi YB; software-oriented job was performed by Qi YB; validation was done by Yu WJ; formal analysis was performed by Qi YB and Yu DS; investigation was done by Guo HX; resources were provided by Pan B; data curation was done Qi YB; writing—original draft preparation was done by Qi YB; writing—review and editing was done by Yu WJ, Qi YB, and Guo HX; supervision was performed by Yu DS; and funding acquisition was done by Yu WJ. All authors have read and agreed to the published version of the manuscript.

Acknowledgments

Thanks to Hunan University of Science and Technology for its strong support to the college and laboratory, as well as the experimental site provided by Guizhou Institute of Technology. In addition, we would like to express our gratitude to Baidu Academic for providing translation software and Hindawi for providing free grammar services. This study was supported by the National Natural Science Foundation of China (grant nos. 52174076 and 51974117) and the Hunan Provincial Natural Science Foundation of China (grant no. 2023JJ30261).

References

[1] W. Yu, B. Pan, F. Zhang, S. Yao, and F. Liu, "Deformation characteristics and determination of optimum supporting time of alteration rock mass in deep mine," *KSCE Journal of Civil Engineering*, vol. 23, no. 11, pp. 4921–4932, 2019.

[2] W. Yu, G. Wu, B. Pan, Q. Wu, and Z. Liao, "Experimental investigation of the mechanical properties of sandstone–coal–bolt specimens with different angles under conventional triaxial compression," *International Journal of Geomechanics*, vol. 21, no. 6, Article ID 04021067, 2021.

[3] G. Zhang, Z. Wang, G. Guo et al., "Study on regional strata movement during deep mining of Erdos Coal Field and its control," *International Journal of Environmental Research and Public Health*, vol. 19, no. 22, Article ID 14902, 2022.

[4] J. Chen, K. Shi, Y. Pu et al., "Study on instability fracture and simulation of surrounding rock induced by fault activation under mining influence," *Rock Mechanics Bulletin*, vol. 2, no. 2, Article ID 100037, 2023.

[5] R. Shan, D. Liu, H. Wang, X. Tong, Z. Li, and Y. Zhao, "Study of the fracture instability and fault slip risk of overlying strata during mining near faults," *Bulletin of Engineering Geology and the Environment*, vol. 82, no. 3, Article ID 94, 2023.

[6] Z. Xiao, S. Gu, Y. Zhang, and H. Wang, "An effective control method of rock burst induced by shear instability of fault structure under complicated geological conditions," *Bulletin of Engineering Geology and the Environment*, vol. 82, no. 4, Article ID 105, 2023.

[7] W. Yu, K. Li, Z. Liu, B. An, P. Wang, and H. Wu, "Mechanical characteristics and deformation control of surrounding rock in weakly cemented siltstone," *Environmental Earth Sciences*, vol. 80, no. 9, pp. 1–15, 2021.

[8] W. Yu, G. Wu, B. Pan, C. Wang, K. Li, and Z. Liao, "Laboratory and field investigations of different bolting configurations for coal mine roadways in weak coal strata," *Bulletin of Engineering Geology and the Environment*, vol. 80, no. 12, pp. 8995–9013, 2021.

[9] M. Shahzad, Y. Majeed, M. Z. Emad, M. Arshad, R. Goraya, and M. Akram, "Assessing mechanical characteristics of typical support system being used in thin seam coal mining of Pakistan," *International Journal of Mining and Mineral Engineering*, vol. 13, no. 4, pp. 333–351, 2022.

[10] G. Zhang, G. Guo, Y. Gong, A. Xiao, T. Zhao, and H. Li, "Failure mechanism of giant-thick strata characterized by weak cementation based on superimposed similar material simulation," *KSCE Journal of Civil Engineering*, vol. 26, no. 8, pp. 3355–3369, 2022.

[11] J. Li, B. Fu, H. Zhang, Q. Zhao, and Q. Bu, "Study on fracture behavior of directly covered thick hard roof based on bearing capacity of supports," *Applied Sciences*, vol. 13, no. 4, Article ID 2546, 2023.

[12] H. Wang, J. Wang, D. Elmo, M. He, Z. Ma, and C. Gao, "Ground response mechanism of entries and control methods induced by hard roof in longwall top coal caving panel," *Engineering Failure Analysis*, vol. 144, Article ID 106940, 2023.

[13] J. Bai, S. Duan, R. Liu et al., "Evolution of delayed water inrush in fault fracture zone considering time effect," *Arabian Journal of Geosciences*, vol. 14, no. 11, Article ID 1001, 2021.

[14] P. Zhang, L. Yuan, G. Zhang, Z. Kong, J. Wang, and W. Chen, "Behavior of overlying strata at the working face of in a multi-fault zone," *Geotechnical and Geological Engineering*, vol. 39, no. 2, pp. 691–707, 2021.

[15] Z. Jiao, L. Wang, M. Zhang, and J. Wang, "Numerical simulation of mining-induced stress evolution and fault slip behavior in deep mining," *Advances in Materials Science and Engineering*, vol. 2021, Article ID 8276408, 14 pages, 2021.

[16] T. Lan, J. Sun, AS. Batugin et al., "Dynamic characteristics of fault structure and its controlling impact on rock burst in mines," *Shock and Vibration*, vol. 2021, Article ID 7954876, 7 pages, 2021.

[17] J. Zhang, L. Guo, W. Mu, S. Liu, and D. Zhao, "Water-inrush risk through fault zones with multiple karst aquifers underlying

the coal floor: a case study in the Liuzhuang Coal Mine, Southern China," *Mine Water and the Environment*, vol. 40, no. 4, pp. 1037–1047, 2021.

[18] H. Wang, Y. Jiang, C. Jiang, J. Di, and Y. Liu, "Characteristics of overlying strata movement in double fault area under the dynamic pressure," *Journal of Mining and Safety Engineering*, vol. 03, pp. 513–518, (in Chinese), 2019.

[19] N. N. Danesh, Y. Zhao, T. Teng, and M. S. Masoudian, "Prediction of interactive effects of CBM production, faulting stress regime, and fault in coal reservoir: numerical simulation," *Journal of Natural Gas Science and Engineering*, vol. 99, Article ID 104419, 2022.

[20] P. Kong, A. Yuan, Y. Liu, and Z. Li, "Study on fault slip dynamic response and rock burst potential under the influence of different horizontal stresses," *Geomatics, Natural Hazards and Risk*, vol. 13, no. 1, pp. 1321–1341, 2022.

[21] Y. Guo, L. Luo, and C. Wang, "Research on fault activation and its influencing factors on the barrier effect of rock mass movement induced by mining," *Applied Sciences*, vol. 13, no. 1, Article ID 651, 2023.

[22] M. Kruszewski, G. Montegrossi, M. Balcewicz et al., "3D in situ stress state modelling and fault reactivation risk exemplified in the Ruhr Region (Germany)," *Geomechanics for Energy and the Environment*, vol. 32, Article ID 100386, 2022.

[23] S. R. Islavath, S. Katkuri, D. Deb, and H. Kumar, "Negotiating an inclined normal fault in a longwall panel: a case study," *International Journal of Coal Geology*, vol. 251, Article ID 103935, 2022.

[24] P. Wang, L.-S. Jiang, P.-Q. Zheng, G.-P. Qin, and C. Zhang, "Inducing mode analysis of rock burst in fault-affected zone with a hard–thick stratum occurrence," *Environmental Earth Sciences*, vol. 78, no. 15, pp. 1–13, 2019.

[25] X. Zhang, H. Wang, M. Yang, L. Han, and J. Liu, "Analysis of the influence mechanism of small fault activation under the influence of mining at deep coal faces," *ACS Omega*, vol. 7, no. 41, pp. 36836–36847, 2022.

[26] N. Tan, R. Yang, and Z. Tan, "Influence of complicated faults on the differentiation and accumulation of in-situ stress in deep rock mass," *International Journal of Minerals, Metallurgy and Materials*, vol. 30, no. 5, pp. 791–801, 2023.

[27] L. Dou, Z. Sun, X. Li, Q. Liu, S. Gong, and C. Wang, "Detection and targeted control of regional stress field for coal burst prevention," *Geohazard Mechanics*, vol. 1, no. 1, pp. 69–76, 2023.

[28] J. Chen, Y. Zhang, K. Ma, D. Tang, H. Li, and C. Zhang, "Analysis of mining crack evolution in deep floor rock mass with fault," *Geofluids*, vol. 2021, Article ID 5583877, 15 pages, 2021.

[29] L. Zhang, L. Xu, Z. Wei, and C. Feng, "Study on in-seam wave response characteristics of reflection in fault bearing coal seam of Shuangliu Coal Mine," *Geotechnical and Geological Engineering*, vol. 40, no. 1, pp. 395–404, 2022.

[30] K. Wang, L. Wang, and B. Ren, "Failure mechanism analysis and support technology for roadway tunnel in fault fracture zone: a case study," *Energies*, vol. 14, no. 13, Article ID 3767, 2021.

[31] M. Qian, P. Shi, and J. Xu, *Ground Pressure and Ground Control*, China University of Mining and Technology Press, Xuzhou, China, (in Chinese), 2010.

[32] W. Fangtian, "*Overlying strata movement laws and ground control of the longwall face mining in a shallow depth seam in proximity beneath a room mining goaf*," PhD Thesis (in Chinese), China University of Mining and Technology, Xuzhou, China, 2012.

[33] Y. Xu, S. Liu J. Li, and L. Zhou, "Calculation formula and applicability analysis of the height of the "two zones" overburden rock in fully mechanized caving mining," *Coal Mining*, vol. 2, pp. 4–7, (in Chinese), 2011.

[34] Y. Wu, Y. Guan, S. Wang, and W. Liu, "Study on the proportion of similar materials," *Journal of Fuxin Mining Institute*, vol. 01, pp. 32–49, (in Chinese), 1981.

[35] C. Mu and Y. Liu, "Study on gas comprehensive control technology in steep and extra thick coal seam," in *IOP Conference Series: Earth and Environmental Science*, vol. 768, IOP Publishing, 2021.